Catalysis Today 334 (2019) 24–29

Contents lists available at ScienceDirect

Catalysis Today

journal homepage: www.elsevier.com/locate/cattod

Preparation of magnetically recoverable carbon nanotube-supported Pd(II) catalyst

Antonin Desmecht[a], Florence Pennetreau[a], Anaëlle L'hoost[a], Irina Nircha[a], Benoit P. Pichon[b], Olivier Riant[a], Sophie Hermans[a,*]

[a] Institute of Condensed Matter and Nanosciences (IMCN), Université catholique de Louvain, Place Louis Pasteur 1, 1348, Louvain-la-Neuve, Belgium
[b] Université de Strasbourg, CNRS, Institut de Physique et Chimie des Matériaux de Strasbourg, UMR 7504, F-67000, Strasbourg, France

ARTICLE INFO

Keywords:
Immobilized Pd catalyst
Magnetic support
Suzuki cross-coupling
Carbon nanotubes
Functionalization

ABSTRACT

Multi-walled carbon nanotubes were filled or externally decorated with iron oxide nanoparticles to make them magnetically-recoverable. In the first case, the external surface was treated to be free of defects and oxygenated groups to favor internalization. A thermal decomposition route was followed in the second case. The formed nanoparticles were characterized and shown to consist in magnetite and/or maghemite. Moreover, when placed on the external surface of carbon nanotubes, they remained small and well-dispersed, leaving high proportion of free carbon surface for further functionalization. The intact sp^2 carbon atoms were subsequently attacked by means of xanthate radical chemistry, followed by post-functionalization to graft a dipyridylamine ligand on the surface of both solids and pristine carbon nanotubes for comparison. Solids at each step of the syntheses were characterized by X-ray photoelectron spectroscopy (XPS). Palladium coordination onto the surface ligand was studied and the precursor $[Pd(COD)Cl_2]$ complex gave the best results to afford CNT-supported molecular Pd(II) catalysts. XPS confirmed the +2 oxidation state of palladium on the carbon surface. The so-prepared magnetically-recoverable catalysts were successfully used in Suzuki-Miyaura cross-coupling catalytic application.

1. Introduction

In our modern society demanding more economically and ecologically-viable processes, the development of supported catalysts has been the central point of many researches. Carbonaceous materials have always been considered as good candidates for the preparation of supported catalysts [1–4]. Yet, commonly used carbonaceous supports still suffer from different drawbacks such as the presence of various impurities which can act as catalyst poisons or a microporous structure leading to mass-transfer limitations. In addition, the difficulty of spectroscopic characterization may result in a lack of fundamental understanding. To overcome these issues, nano-carbons have been envisaged as an alternative in the design of supported catalysts [5,6]. In particular, due to their outstanding properties such as high surface area and high chemical and thermal stabilities, carbon nanotubes (CNTs) have been studied as catalyst supports [7,8]. Most of the examples presented in the literature concern the anchoring of metallic nanoparticles on their outer walls [7,8]. To a far lesser extent, examples of supported molecular complexes have also been described [6]. These allow fine-tuning of selectivity but are more complicated to synthesize. However, in all cases, the use of CNTs as solid supports requires a filtration step that demands particular nanofiltration units and therefore is tedious and time-consuming. In parallel, the advantage of using magnetically recoverable supports has already been reported [9–12]. Hence we propose here to make CNTs magnetically recoverable to overcome the filtration issue. We prepared magnetic CNTs (Mag-CNTs) using iron oxide nanoparticles either by decorating their external surface with iron oxide nanoparticles (Fe-CNTs) or by filling their internal cavity (Fe@CNTs). As far as we are aware, no example of molecular metal catalyst supported on magnetically recoverable CNTs have been reported so far. In this context, we prepared as a proof of concept a structurally well-defined palladium complex supported on Mag-CNT as easily recoverable homogeneous catalyst.

Suzuki-Miyaura cross-coupling (SMCC) reaction [13] is considered as one of the most useful reactions in today organic synthesis [14,15]. In this paper, Fe-CNTs and Fe@CNTs (and pristine CNTs for comparison) have been covalently functionalized to anchor Pd(II) complexes in order to be tested as catalysts for the SMCC reaction. Of particular importance is the choice of the functionalization method. The Mag-CNTs cannot be exposed to harsh conditions without taking the risk of

* Corresponding author.
E-mail address: sophie.hermans@uclouvain.be (S. Hermans).

https://doi.org/10.1016/j.cattod.2019.02.057
Received 14 July 2018; Received in revised form 14 December 2018; Accepted 22 February 2019
Available online 27 February 2019
0920-5861/

releasing the iron oxide nanoparticles which fill or decorate the nanotubes. For this reason, a soft covalent functionalization method was selected: the covalent grafting of xanthate compounds in presence of peroxide as radical initiator. This method has been proven efficient to produce functionalized CNTs [16] and graphene [17] samples without visible damages.

It should be underlined that Suzuki-Miyaura cross-coupling is used mainly for fine chemistry applications, for example pharmaceuticals synthesis. Industrial processes making use of such reaction exist at the multi-kilogram scale [18]. However, as in most homogeneously-catalyzed processes, the palladium soluble species catalyzing the reaction are not recovered and reused. Even worse, the workup necessary to isolate and purify the final product leads to inactivation and elimination of catalysts in the waste. Moreover, in the case of APIs (Active Pharmaceutical Ingredients), very strict limits are specified for residues of (toxic) metals. Hence, additional methods for Pd scavenging are being developed at the industrial scale, using for example resins functionalized by thiols or amine ligands [19] to reach < 100 ppm Pd levels. Hence there is high scope for developing methods to immobilize homogeneous catalysts onto solid supports that allow straightforward recovery and recycling.

2. Experimental

2.1. Materials and methods

2.1.1. Chemicals

All chemicals were used as received except AcOEt and dichloromethane that were dried over CaH_2 and P_2O_5 respectively, distilled under argon and stored under argon atmosphere over molecular sieves. Tetrahydrofuran (THF) was dried over Na/benzophenone, distilled under argon and used directly. Thin-MWCNTs were received from Nanocyl (95+ wt.% carbon pure, research grade, Product Ref.: NC-3100) and were used without further purification. Large-MWCNTs were purchased from Pyrograf Products (hollow vapor-grown multi-walled CNTs; Product Ref.: CNT19, Pyrograf Products). Silica gel for column chromatography was ROCC 60 (40–63 μm).

2.1.2. Instrumental

2.1.2.1. X-ray photoelectron spectroscopy (XPS). XPS analyses were carried out at room temperature with a SSI-X-probe (SSX 100/206) photoelectron spectrometer from Surface Science Instruments (USA) equipped with a monochromatized microfocus Al X-ray source. Samples were stuck onto small sample holders with double-face adhesive tape and then placed on an insulating ceramic carousel (Macor®, Switzerland). Charge effects were avoided by placing a nickel grid above the samples and using a flood gun set at 8 eV. The energy scale was calibrated with reference to the Au $4f_{7/2}$ peak at 84 eV and the binding energies were calculated with respect to the C-(C,H) component of the C 1s peak fixed at 284.8 eV. Data treatment was performed using the CasaXPS program (Casa Software Ltd., UK). The peaks were decomposed into a sum of Gaussian/Lorentzian (85/15) after subtraction of a Shirley-type baseline.

2.1.2.2. Nuclear magnetic resonance (NMR). All ^{1}H, ^{13}C and ^{19}F NMR spectra were recorded in $CDCl_3$ solution with tetramethylsilane (TMS) as internal standard, at ambient temperature on a Avance 300 MHz Bruker Fourier Transform Spectrometer operating at 300 MHz for ^{1}H, 75 MHz for ^{13}C and 282 MHz for ^{19}F. All the spectra were calibrated at δ = 0.00 ppm (TMS) and with the $CDCl_3$ peak fixed at δ = 7.26 ppm for ^{1}H and δ = 77.16 ppm for ^{13}C. Spectral features are quoted as follows: s = singulet, d = doublet, t = triplet, q = quartet and m = multiplet.

2.1.2.3. High-Resolution mass spectrometry (HR-MS). HR-MS measurements were performed on a Q-Extractive Orbitrap from Thermofisher with ionization by APCI.

2.1.2.4. Thermogravimetric analysis. Thermograms were recorded on a TGA/SDTA 851^{e} from Mettler Toledo. Samples (2–5 mg) were heated at 10 °C/min under a nitrogen flux in alumina containers.

2.1.2.5. Transmission electron microscopy (TEM). TEM images were obtained with a LEO922 equipped with an OMEGA energy filter. Samples suspended in hexane were drop casted on a holey carbon film supported on a copper grid. To visualize lattice fringes of magnetic nanoparticles, samples were characterized by HR-TEM with a TOPCON 002B microscope operating at 200 kV (point resolution 0.18 nm).

2.1.2.6. Infrared spectroscopy (IR). Infrared spectra of xanthates were recorded in KBr pellets on a BRUKER EQUINOX 55 spectrometer in transmission mode.

2.1.2.7. Gas chromatography (GC). Chromatographs were recorded on a GC trace, Finnigan Mat equipped with an AS-3000 Autosampler (FID detector). The GC column is a Chirasil-Dex CB (30 m x 25 mm x 0.25 μm (Agilent)). The parameters used were fixed as follows: the gas vector is He (1.2 ml/min), the "injector split/split less" ratio is of 1/30. The internal standard used is dodecane and the temperature program is 120 °C (12′)→120 °C to 160 °C (5 °C/min) →160 °C (2′). The main compounds retention time (in minutes) are the following: 4-Iodotoluene = 6.467; Biphenyl = 16.775; 4-Methylbiphenyl = 20.125; Dodecane = 5.375.

2.1.2.8. (Powder) X-ray diffraction (XRD). Samples were introduced into 0.5 mm thin-walled glass capillaries (Hilgenberg GmbH), mounted on a goniometer head and kept at 200 mm from the detector. Diffractograms were then collected at room temperature using a MAR345 diffractometer (MarResearch GmbH), equipped with a Mo-Kα (0.71073 Å) anode and a XENOCS focusing mirror. The obtained 2D diffractograms were azimuthally integrated using the Fit2D software and calibrated with a LaB_6 standard (NIST 660b Standard).

2.2. Syntheses

Fe@CNTs [20], xanthate [16] (R.N. 1428628-77-6) and dipyridylamine ligand [21] (R.N. 1417745-31-3) were synthesized following literature procedures.

2.2.1. Fe-CNTs preparation [22,23]

Thin-CNTs (30 mg) were suspended in triethylene glycol (10 ml) and sonicated for 15 min. Iron (III) acetylacetonate (60 mg) was added together with 5 ml of triethylene glycol. The suspension was transferred into a 250 ml autoclave (Stainless steel autoclave Parr instrument) where it was heated to 250 °C in 80 min and maintained at 250 °C for 40 min. After naturally cooling to room temperature, MeOH (30 ml) was added and the suspension was centrifuged 10 min at 4000 rpm (Universal 320 from Hettich). The supernatant was eliminated and the carbon nanotubes washed with MeOH and water and finally dried under vacuum.

2.2.2. CNTs covalent functionalization

In a typical reaction, CNTs (24 mg, 2 mmol of C; 1 equiv.) were introduced in a three-neck round bottom flask and dried in an oil bath at 100 °C, under vacuum, overnight. Distilled ethyl acetate (10 ml) was added under argon and the flask content was sonicated for 1 h. Afterwards, the solution was heated under reflux in a 100 °C oil bath and the entire xanthate amount and half of the radical initiator (Dilauroyl peroxide, DLP) were added with a few milliliters of AcOEt. After 3 h, the second half of the DLP and a few milliliters of AcOEt were added and the solution was heated for an additional 3 h. The crude mixture was stirred at room temperature overnight. The solution was filtered (on PVDF membrane, 0.22 μm pore size) and the solid was washed successively with ethanol (100 ml), tetrahydrofurane (100 ml),

ethyl acetate (100 ml) and diethylether (100 ml). The functionalized CNTs (noted **X**-CNTs) were finally suspended in AcOEt (10 ml), sonicated for 1 h before being washed as before and dried under vacuum at room temperature overnight.

2.2.3. Dipyridylamine ligand grafting

140 mg of **X**-CNTs were introduced in a Schlenk round bottom flask under argon. Distilled DCM (25 ml) was added and the resulting suspension was sonicated for 60 min. Dipyridylamine ligand (280 mg – 2 wt. equivalent) was added and the suspension was stirred for 24 h at room temperature. Nanotubes were collected by filtration on PVDF membrane (0.22 µm pore size) and washed with DCM (200 ml), EtOH (100 ml) and diethyl ether (100 ml). The solid was finally suspended in DCM, sonicated for 60 min, washed as previously and dried under vacuum at room temperature. The obtained nanotubes with ligands at their surfaces are noted NˆN-CNTs.

2.2.4. Palladium anchoring

120 mg of NˆN-CNTs were introduced in a Schlenk round bottom flask under argon. Distilled DCM was added and the suspension was sonicated for 60 min. Palladium complex [$Pd(COD)Cl_2$] (140 mg – 1 wt. equivalent) was added and the reactive medium stirred at room temperature for 3 h. Non-coordinated palladium complex was removed by filtration (on PVDF membrane, 0.22 µm pore size), followed by washings with DCM, sonication for 10 min and new DCM washings. The solid was finally recovered and dried at room temperature.

2.2.5. Suzuki-Miyaura cross-coupling

The palladium catalyst and DMF (10 ml) were introduced in a three-neck round bottom flask and sonicated for 1 h. Iodotoluene (218.03 mg, 1 mmol), phenylboronic acid (182.89 mg, 1 mmol), K_2CO_3 (414.63 mg, 3 mmol) and DMF (5 ml) were added and the suspension heated at 120 °C. Samplings for GC measurements were performed as follows: a small fraction of the reaction media is taken out of the three-neck flask and filtrated. The DMF solution is introduced in a flask containing 2 ml of water and 2 ml of DCM. After phase separation, the organic phase is collected, dried on $MgSO_4$ and introduced in a 5 ml volumetric flask. The flask is completed with 0.5 ml of dodecane solution (2 vol. % in DCM) and DCM.

For recycling, the reaction medium at the end of the test was contacted with an external magnet and the supernatant was removed (magnetic decantation). The solid was re-suspended in another solvent for washing and the solid was isolated again by magnetic decantation. This cycle of washing/magnetic decantation was repeated several times, using the following sequence of solvents: DMF, H_2O twice, acetone, ether. The solid catalyst was then dried under vacuum.

3. Results and discussion

CNTs filled with iron oxide nanoparticles (Fe@CNTs, Fig. 1) have been synthesized as we have previously reported [20]. The residual iron coming from CNT (Pyrograf Products CNT19) synthesis catalysts was first removed by an acidic treatment. Removal of the oxygenated functions at CNT surface (to avoid any adsorption of nanoparticles on their external surface) is also necessary to afford the selective filling of CNT. Finally CNTs were filled up to 50 wt% with 13 nm sized iron oxide nanoparticles by thermal decomposition of iron stearate in octadecene. HR-TEM images (Fig. 1(c,d)) show the lattice fringes of the obtained nanoparticles, that can be indexed to the hkl planes of iron oxide spinel structure. CNTs bearing iron oxide NPs on the external surface (Fe-CNTs, Fig. 1(a)) have been prepared by heating a suspension of *thin*CNTs (Nanocyl NC3100) and $Fe(acac)_3$ in triethylene glycol in an autoclave [22,23]. The obtained Fe@CNTs and Fe-CNTs have been characterized by XPS, XRD and TEM. XPS spectra of Fe-CNTs (Fig. 2) and Fe@CNTs (Fig. S2 in ESI) confirmed the presence of carbon, oxygen and iron in the composites (Fig. 2-left). Furthermore the binding energy

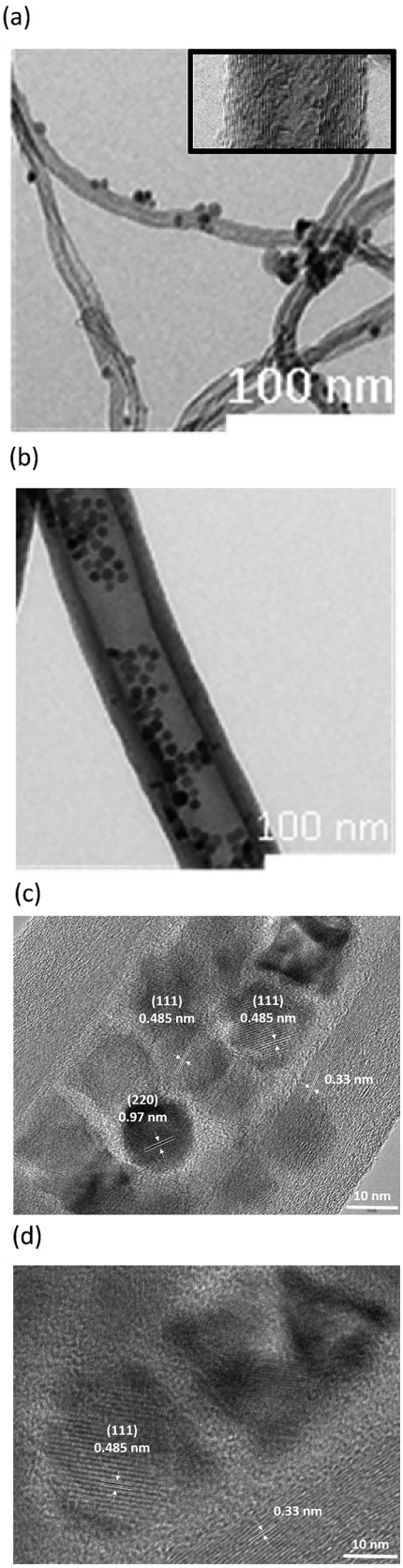

Fig. 1. TEM micrographs of Fe-CNTs (a) and Fe@CNTs (b). Inset in (a) shows zoom on CNTs walls. HR-TEM images of Fe@CNTs (c) show lattice fringes of magnetic nanoparticles (hkl planes corresponding to spinel structure of iron oxide) and zoom (d) also show walls of CNTs with typical interlayer spacing.

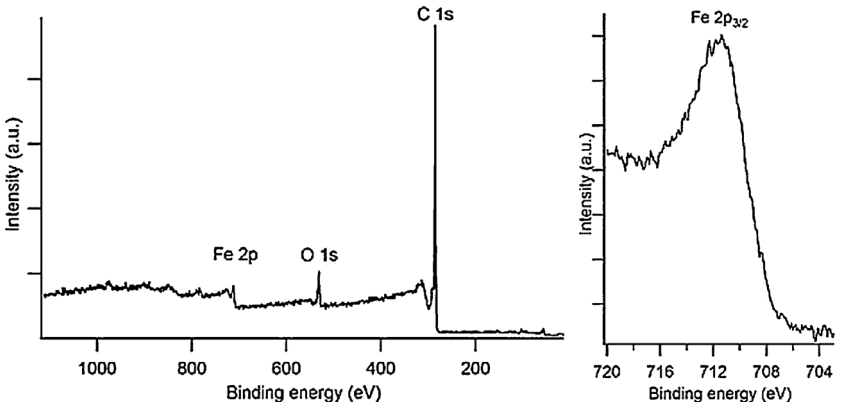

Fig. 2. XPS spectra of Fe-CNTs: General (left) and Fe $2p_{3/2}$ (right) spectra.

at which the iron Fe $2p_{3/2}$ peaks arises (711.5 eV, Fig. 2-right) indicates the formation of an iron oxide phase (likely to be maghemite (Fe_2O_3) and/or magnetite (Fe_3O_4) [24]. It is worth noting that no iron peak is detected in the pristine *thin*CNTs XPS spectrum (see Fig. S1 in ESI).

Pristine *thin*CNTs (inset Fig. 3), Fe-CNTs (Fig. 3) and Fe@CNTs (see Fig. S3 in ESI) were also characterized by powder XRD. Pristine *thin*CNTs diffractogram is characterized by the typical graphite-like diffraction peak due to organization in the nanotubes structure. After nanoparticles incorporation, new diffraction peaks appeared, which match well the ones referenced for magnetite, confirming XPS results. However, under air, magnetite has a high tendency to get oxidized to maghemite but magnetite and maghemite phases present highly similar diffractograms, hence the presence of the latter cannot be ruled out as a minor phase. In any case the possible cohabitation of phases in not a problem because both are magnetic. Finally, the peak broadening indicates the presence of small nanoparticles in the sample, in agreement with TEM observations.

Detailed magnetic characterization of Fe@CNTs is reported in [25]: Magnetization curves as a function of an applied field at 300 K display a hysteretic behavior consistent with superparamagnetic nanoparticles above their blocking temperature. Moreover, the nanoparticles were found to consist of a magnetite core surrounded by an oxidized shell. Given the small sizes of nanoparticles obtained in Fe-CNTs, they also are superparamagnetic as highlighted by SQUID magnetometry [26] for similar solvothermally-prepared samples.

The micrographs of Fe-CNTs sample reveal the presence of small nanoparticles dispersed at the external surface of the CNTs (Fig. 1 (a)). By opposition, Fe@CNTs sample visualization confirms the iron oxide nanoparticles incorporation inside the tubular central cavities of the CNTs. Both present magnetic nanoparticles of small and uniform sizes (mean diameter: 7 nm on Fe-CNTs versus 13 nm in Fe@CNTs as seen in HR-TEM micrographs, Fig. 1 (c,d)), albeit the different diameter of CNT used in each case (~20 nm for Fe-CNTs and ~70 nm for Fe@CNTs). TEM images at higher magnification (Fig. 1) also show that the nanotube general cylindrical structures and concentric walls structure have not been damaged during the iron oxide incorporation processes, again in both cases.

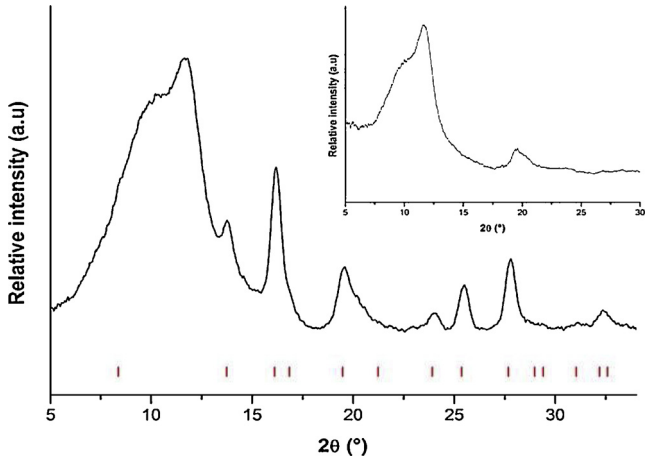

Fig. 3. XRD difractogram of Fe-CNTs. Solid line: experimental data, red hyphens: magnetite Bragg reflections. (Inset: *thin*CNTs difractogram).

*Thin*CNTs, Fe@CNTs and Fe-CNTs have been covalently functionalized using xanthate-arising radicals in presence of a peroxide as radical initiator (Fig. 4). This method has already been proven to be effective to functionalize pristine CNTs with organic functions [16,17]. The same methodology has therefore been applied to magnetic carbon nanotubes. The selected xanthate (noted **X**) bearing an activated ester function has been chosen in order to use it as an anchoring point to tether a palladium (II) complex in a subsequent step.

The functionalized samples have been analyzed by XPS to determine the functionalization yield. Results are gathered in Table 1. Those results show that the xanthate grafting occurred at both Fe-CNTs and Fe@CNTs surfaces as sulfur and fluorine arising from xanthate-coming moieties are detected. As previously reported, the sulfured part of the xanthate is grafted with a much lower yield compared with pentafluorophenol activated ester function [16,17,27]. In addition, as the functionalization involves a peroxide radical initiator, the direct addition of the initiator onto the CNT surface cannot be avoided, but this has also been minimized by adjusting the reactions conditions. Moreover, these grafted species are dead-end surface sites that do not interfere with the subsequent steps. The amount of iron detected in Fe@CNTs is higher than in Fe-CNTs but this should not influence the catalytic performance as it is not the active phase but its role is merely to render the samples magnetic. The amount of fluorine is also higher in this Fe@CNTs sample. This can be explained by two factors: (i) the starting CNT sample is different and (ii) it had been treated to remove surface oxygenated groups on external surface to favor internalization of magnetic nanoparticles, hence it presents more sites for radical attack.

In a second step, functionalized CNT with no magnetic nanoparticles have been post-functionalized to anchor the Pd(II) complex (Fig. 5). First, the activated ester moieties have been reacted with the primary amine of the bifunctional ligand **L**. Secondly, the palladium has been tethered at the nanotube surface by ligand exchange between a precursor Pd(II) soluble complex and the dipyridylamine function of the ligand **L**. Several complexes have been tested in order to obtain the desired product. The XPS results obtained on *thin*CNTs are presented in Table 2.

These XPS results reveal the importance of the starting Pd(II) complex selection in the preparation of the supported catalysts. In view of the target supported catalyst stoichiometry, the theoretical Pd/N atomic ratio is equal to 0.25. Yet catalysts prepared with [$Pd(acac)_2$]

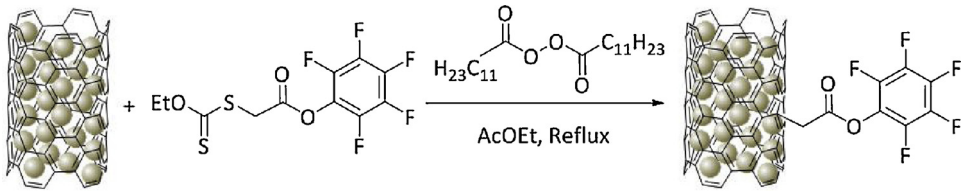

Fig. 4. Radical functionalization of Fe@CNTs with xanthate **X**. Low sulfur content not shown for clarity.

Table 1
XPS characterization of xanthate functionalized nanotubes (nanotubes, xanthate and DLP introduced in a 1/1/1 ratio – See ESI).

	Surface concentrations (atomic %)		
	S2p	F1s	$Fe2p_{3/2}$
X-thinCNTs	0.22	1.78	–
X-Fe-CNTs	0.46	2.52	0.79
X-Fe@CNTs	0.41	5.22	1.64

Table 2
XPS characterization of Pd/**L**/**X**/CNTs samples.

Precursor complex	XPS $Pd3d_{5/2}$ peak characteristics		
	Content (at.%)	Position (eV)	Pd/N ratio
$Pd(OAc)_2$	0.31	336.7	0.74
$Pd(CH_3CN)_2Cl_2$	2.40	336.3	5.05
$Pd(COD)Cl_2$	0.14	337.6	0.25

and $[Pd(CH_3CN)_2Cl_2]$ are characterized by a Pd/N ratio higher than the theoretical value. This means that the palladium atoms are not coordinated to ligand **L** as expected but rather, at least partially, adsorbed at the nanotube surface. Pd being a noble metal, it is easily reduced and adsorbed on the electron-rich carbonaceous surface. On the contrary, in the case of $[Pd(COD)Cl_2]$ the Pd/N ratio matches with the theoretical value. In addition, the Pd $3d_{5/2}$ peak position in the XPS spectra is in agreement with palladium at the oxidation state of (+2) (Fig. 6) [24]. Those results confirm the supported palladium complex to be the one expected, only when using $[Pd(COD)Cl_2]$ as precursor. It was therefore chosen for immobilization on the magnetic nanotubes.

The obtained solids have been characterized by XPS and Pd contents of 0.11 at. % and 0.19 at. % were found for Pd^{II}/Fe-CNTs and Pd^{II}/Fe@CNTs, respectively. In both cases, Pd is present in its (+2) oxidation state as expected ($Pd3d_{5/2}$ peak positioned at 337.7 eV in Fe-CNTs and at 337.6 eV in Fe@CNTs supported Pd composites). The presence of magnetic nanoparticles did not hinder the immobilization of the catalytic complex. It is worth noting that Pd/Fe-CNTs and Pd/Fe@CNTs still respond to external magnetic fields.

To prove the validity of our immobilization method, some of the prepared catalysts have been tested in the Suzuki-Miyaura cross-coupling between 4-iodotoluene and phenylboronic acid (Fig. 7). For this purpose, Pd^{II}/*thin*CNTs and Pd^{II}/Fe-CNTs have been analyzed by bulk elemental analysis to determine the Pd mass loadings and calculate catalytic amounts to engage in tests. Values of 0.69 wt. % and 0.60 wt. % were found for catalysts supported on CNTs and Fe-CNTs, respectively.

First, blank catalytic tests were performed using *thin*CNTs and Fe-CNTs as catalysts in order to preclude any activity of the supports in the cross-coupling reaction. No conversion was obtained in these tests. Then, using nanotubes-supported Pd^{II} complexes as catalysts, the conversion of 4-iodobenzene in 4-methylbiphenyl and biphenyl was observed. The prepared magnetic nanotubes are easily dispersed in DMF (Fig. 8, left). The use of Pd^{II}/*thin*CNTs and Pd^{II}/Fe-CNTs gave rise to 4-iodotoluene conversion of 77% and 58% respectively. After catalytic reaction, the solid Pd^{II}/Fe-CNTs have been straightforwardly separated magnetically from the liquid reaction medium, as when approaching a magnet the solid readily segregates from the solution within a few seconds (see Fig. 8, right). After solvent washings, it can easily be reused.

4. Conclusion

To summarize, we have prepared nanotubes-supported palladium catalysts. The supports used were pristine carbon nanotubes (*thin*CNTs) and nanotubes bearing iron oxide magnetic nanoparticles inside (Fe@CNTs) or outside (Fe-CNTs) their tubular structures. Those nanotubes have first been covalently functionalized with xanthate-coming radicals before the anchoring of a dipyridilamine ligand and palladium complexation. The presence of magnetic nanoparticles decorating or filling the CNTs was not found to hinder the immobilization process. The as-obtained homogeneous supported catalysts have been successfully tested in the Suzuki-Miyaura cross-coupling reaction. At the end of the reaction, the magnetic catalysts are recovered by the simple use of a magnet.

Acknowledgements

The authors thank the F.R.S.-FNRS (Fonds de la Recherche Scientifique) and FRIA (Fonds pour la formation à la Recherche dans l'Industrie et dans l'Agriculture) for funding, as well as Jean-François Statsyns for technical assistance.

Appendix A. Supplementary data

Supplementary data associated with this article can be found, in the online version, at https://doi.org/10.1016/j.cattod.2019.02.057.

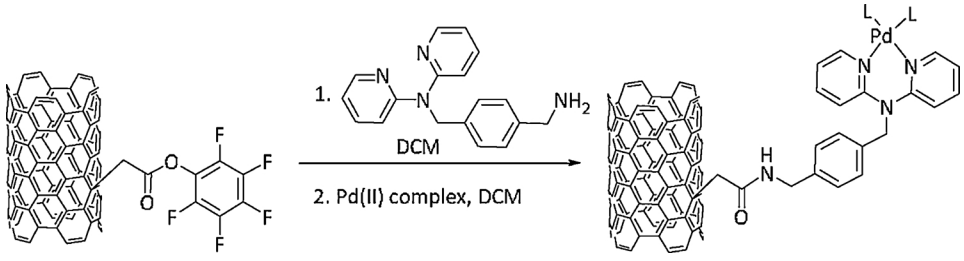

Fig. 5. Pd^{II} complex anchoring on **X**-*thin*CNTs.

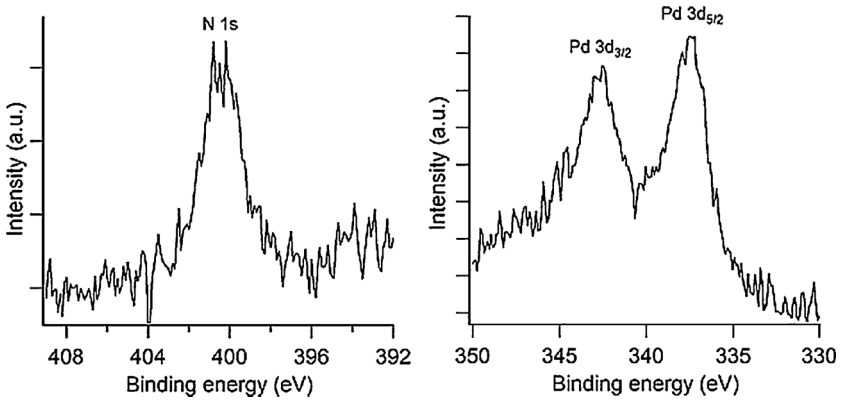

Fig. 6. N 1 s and Pd 3d XPS spectra of Pd^{II}/*thin*CNTs.

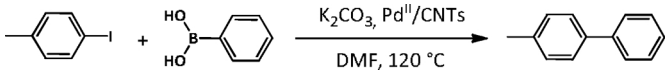

Fig. 7. Suzuki-Miyaura cross-coupling reaction catalyzed by nanotube-supported Pd^{II} complex.

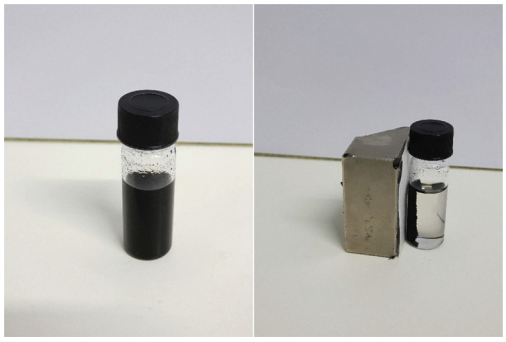

Fig. 8. Dispersion of Fe-CNTs in DMF (left) and response to a magnet (right).

References

[1] V. Calvino-Casilda, A.J. López-Peinado, C.J. Durán-Valle, R.M. Martín-Aranda, Catal. Rev. 52 (2010) 325–380.
[2] H. Jüntgen, Fuel 65 (1986) 1436-1146.
[3] E. Lam, J.H.T. Luong, ACS Catal. 4 (2014) 3393–3410.
[4] E. Auer, A. Freund, J. Pietsch, T. Tacke, Appl. Catal. A-Gen. 173 (1998) 259–271.
[5] D.S. Su, S. Perathoner, G. Centi, Chem. Rev. 113 (2013) 5782–5816.
[6] A. Schaetz, M. Zeltner, W.J. Stark, ACS Catal. 2 (2012) 1267–1284.
[7] D. Vairavapandian, P. Vichchulada, M.D. Lay, Anal. Chim. Acta 626 (2008) 119–129.
[8] Y. Yan, J. Miao, Z. Yang, F.-X. Xiao, H.B. Yang, B. Liu, Y. Yang, Chem. Soc. Rev. 44 (2015) 3295–3346.
[9] R.B.N. Baig, R.S. Varma, Chem. Commun. 49 (2013) 752–770.
[10] V. Polshettiwar, R. Luque, A. Fihri, H. Zhu, M. Bouhrara, J.-M. Basset, Chem. Rev. 111 (2011) 3036–3075.
[11] L.M. Rossi, N.J.S. Costa, F.P. Silva, R. Wojcieszak, Green Chem. 16 (2014) 2906–2933.
[12] S. Shylesh, V. Schünemann, W.R. Thiel, Angew. Chem. Int. Ed. 49 (2010) 3428–3459.
[13] N. Miyaura, T. Yanagi, A. Suzuki, Synth. Commun. 11 (1981) 513–519.
[14] S. Kotha, K. Lahiri, D. Kashinath, Tetrahedron 58 (2002) 9633–9695.
[15] B.W. Glasspoole, E.C. Keske, C.M. Crudden, RSC Catal. Ser. 21 (2015) 521–550.
[16] B. Vanhorenbeke, C. Vriamont, F. Pennetreau, M. Devillers, O. Riant, S. Hermans, Chem. Eur. J. 19 (2013) 852–856.
[17] F. Pennetreau, O. Riant, S. Hermans, Chem. Eur. J. 20 (2014) 15009–15012.
[18] J. Magano, J.R. Dunetz, Chem. Rev. 111 (2011) 2177–2250.
[19] J. Recho, R.J.G. Black, C. North, J.E. Ward, R.D. Wilkes, Org. Process Res. Dev. 18 (2014) 626–635.
[20] W. Baaziz, X. Liu, I. Florea, S. Begin-Colin, B.P. Pichon, C. Ulhaq, O. Ersen, M. Soria-Sánchez, S. Zafeiratos, I. Janowska, D. Begin, C. Pham-Huu, J. Mater. Chem. A 1 (2013) 13853–13861.
[21] A.E. Fernandes, A. Dirani, C. d'Haese, G. Deumer, G. Guo, P. Hensenne, F. Nahra, X. Laloyaux, V. Haufroid, B. Nysten, O. Riant, A.M. Jonas, Chem. Eur. J. 18 (2012) 16226–16233.
[22] H. Wang, L. Cao, S. Yan, N. Huang, Z. Xiao, Mater. Sci. Eng. B 164 (2009) 191–194.
[23] J. Wan, W. Cai, J. Feng, X. Meng, E. Liu, J. Mater. Chem. 17 (2007) 1188–1192.
[24] C.D. Wagner, W.M. Riggs, L.E. Davis, J.F. Moulder, G.E. Muilenberg, Handbook of X-ray Photoelectron Spectroscopy, Perkin-Elmer Corporation, (1979), pp. 29–178 Chapter 2.
[25] W. Baaziz, B.P. Pichon, S. Fleutot, Y. Liu, C. Lefevre, J.-M. Greneche, M. Toumi, T. Mhiri, S. Begin-Colin, J. Phys. Chem. C 118 (2014) 3795–3810.
[26] F. Mederos-Henry, B.P. Pichon, Y. Tchuitio Yagang, A. Delcorte, C. Bailly, I. Huynen, S. Hermans, J. Mater. Chem. C 4 (2016) 3290–3303.
[27] F. Pennetreau, C. Vriamont, B. Vanhorenbeke, O. Riant, S. Hermans, Eur. J. Org. Chem. (2015) 1804–1810.